Eur Biophys J (2004) 33: 657–670
DOI 10.1007/s00249-004-0409-0

ARTICLE

**Birgitte Freiesleben De Blasio · Jens-Gustav Iversen
John-Arne Røttingen**

Intercellular calcium signalling in cultured renal epithelia: a theoretical study of synchronization mode and pacemaker activity

Received: 14 November 2003 / Revised: 24 February 2004 / Accepted: 5 April 2004 / Published online: 26 May 2004

Abstract We investigate a two-dimensional lattice model representation of intercellular Ca^{2+} signalling in a population of epithelial cells coupled by gap junctions. The model is based on and compared with Ca^{2+} imaging data from globally bradykinin-stimulated MDCK-I (Madin-Darby canine kidney)-I cell layers. We study large-scale synchronization of relevance to our laboratory experiments. The system is found to express a wealth of dynamics, including quasiperiodic, chaotic and multiply-periodic behaviour for intermediate couplings. We take a particular interest in understanding the role of "pacemaker cells" in the synchronization process. It has been hypothesized that a few highly hormone-sensitive cells control the collective frequency of oscillation, which is close to the natural frequencies (without coupling) of these cells. The model behaviour is consistent with the conjectures of the pacemaker cell hypothesis near the critical coupling where the cells lock onto a single frequency. However, the simulations predict that the frequency in globally connected systems decreases with increasing coupling. It is found that a pacemaker is not defined by its natural frequency alone, but that other intrinsic or local factors must be considered. Inclusion of partly sensitized cells that do not oscillate autonomously in the cell layer increases the coupling necessary for global synchronization. For not excessively high coupling, these cells oscillate irregularly and with distinctive lower frequencies. In summary, the present study shows that the frequency of synchronized oscillations is not dictated by one or few fast-responding cells. The collective frequency is the result of a two-way communication between the phase-advanced pacemaker and its environment.

Keywords Intercellular calcium signalling · Cultured renal epithelia · Synchronization mode · Pacemaker activity · Intracellular calcium stores

B. F. De Blasio
The Niels Bohr Institute, University of Copenhagen, Copenhagen, Denmark

B. F. De Blasio
Department of Physics, University of Oslo, Oslo, Norway

B. F. De Blasio · J.-G. Iversen · J.-A. Røttingen
Laboratory for Intracellular Signalling,
Department of Physiology, University of Oslo, Oslo, Norway

B. F. De Blasio (✉) · J.-A. Røttingen
Department of Nutrition, Institute of Basic Medical Sciences,
University of Oslo, P.O. Box 1046 Blindern,
0316 Oslo, Norway
E-mail: birgitte.deblasio@medisin.uio.no
Tel.: +47-22-851024
Fax: +47-22-851313

Introduction

Calcium (Ca^{2+}) is a key signalling molecule that is involved in regulating numerous cellular processes and functions (Berridge et al. 1998; Rottingen and Iversen 2000; Berridge 2001). The signals are generated by a variety of mechanisms in different cell types (Jaffe 1993). Many cells also exhibit intercellular Ca^{2+} oscillations with a high degree of spatial synchronicity, which may serve to coordinate cellular activities within a tissue. The signal transmission from one cell to another often depends critically on the presence of intact gap junction channels (Sanderson et al. 1990; Isakson et al. 2001), but may also involve secretion of extracellular messengers (Hassinger et al. 1996; Hofer et al. 2000; Klepeis et al. 2001).

In the heart, intercellular Ca^{2+} waves are highly synchronized and originate in anatomically well-defined pacemaker cells, from where they propagate as action potentials along specific directions (Boyett et al. 2000). The rhythmic Ca^{2+} activation is provided by voltage-dependent channels in the cell membrane (DiFrancesco 1991), which is supported by a Na^{+}–Ca^{2+} exchange current (Huser et al. 2000). As the Ca^{2+} signal in the myocardium arises in response to action potentials, the Ca^{2+} wave spreads much faster than Ca^{2+} signals inside the cells. Epithelia provide another mechanism for the rhythmic activation of Ca^{2+}. Here, the signals are generated by Ca^{2+} release through IP_3-gated Ca^{2+} channels on the endoplasmic reticulum (ER) membrane

(Sanderson 1995). In culture, epithelial pacemakers are characteristically found to be much less spatially organized than their sinoatrial counterparts (Leite et al. 2002). This finding does not necessarily reflect the organization in intact tissue, as, for example, vasopressin-induced Ca^{2+} waves in hepatocytes are found to propagate from pericentral to periportal cells, apparently oriented by a gradient in hormone-receptor expression (Nathanson et al. 1995).

In the renal epithelial MDCK-I cells, synchronous Ca^{2+} signals occur in response to global stimulation with the hormone bradykinin and in the presence of intact gap junctions (Rottingen et al. 1997). It is believed that the intercellular waves emerge due to gap junctional Ca^{2+} diffusion, in resemblance to oscillatory intercellular waves in the blowfly salivary gland (Zimmermann and Walz 1999) and vasopressin-stimulated hepatocytes (Tordjmann et al. 1997; Tordjmann et al. 1998).

Our empirical observations concerning pacemaker cell activity in this cell type have led us to propose the following. (1) Synchronous intercellular Ca^{2+} signalling is coordinated by a few spatially dispersed pacemaker cells in the cell layer. (2) Pacemaker cells are distinguishable from other cells by early Ca^{2+} transients, i.e. by a phase-advance in the Ca^{2+} oscillations. (3) Pacemaker cells are characterized by having a relatively increased hormone sensitivity, implying that they oscillate with the fastest internal frequencies when the cells are uncoupled. (4) The collective frequency of oscillation is close to the internal frequency of the pacemaker cells. (5) The intercellular Ca^{2+} signals are communicated to adjoining cells through gap junctions and spread throughout the tissue in all directions. In the following, we shall refer to the above-mentioned points (1)–(5) as the pacemaker cell hypothesis (PCH).

The observation of synchronous Ca^{2+} oscillations in renal epithelial cells may be regarded as a model for hormonal stimulation of epithelial tissue in general. In particular, experimental data show highly heterogeneous single-cell Ca^{2+} responses. The interplay between cell heterogeneity, collective frequency and pacemaker cell activity is far from clear. We will here investigate signal synchronization in a population of MDCK cells with use of a lattice stochastic model. The simulations are compared with data from globally bradykinin-stimulated MDCK-I cell layers, and the results are compared with previous work.

The model

We use a model by Hofer (1999) to describe the single-cell Ca^{2+} dynamics. The model considers three Ca^{2+} pools: (1) the cytosolic free-Ca^{2+} concentration $[Ca^{2+}]_{cyt}$, denoted by the variable x, (2) the concentration of unbound calcium in the ER $[Ca^{2+}]_{ER}$, described by the variable y and (3) the extracellular Ca^{2+} concentration, which is taken to be constant. The total concentration of free Ca^{2+} in the cell is described with a variable z, given by:

$$z = x + \frac{V_{ER}}{V_{cyt}} y \tag{1}$$

where V_{ER} and V_{cyt} define the "effective" volumes of the ER and the cytosol. The effective volumes are found by rescaling the volumes to incorporate effects from a single type of uniformly distributed buffer. Importantly, the IP_3 level is not considered as a separate variable, but is assumed to be in a quasisteady state, i.e. following the dynamics of active phospho-lipase C (PLC) induced by the hormone stimulation. Cell-to-cell communication is based on gap junctional Ca^{2+} diffusion. No IP_3 exchange between cells is considered. IP_3 diffusion plays a pivotal role for the establishment of intercellular waves in mechanically stimulated systems (Sanderson 1995). Here, IP_3 is necessary to sensitize IP_3R channels as the wave propagates from a single stimulated cell into non-excited cells. However, in globally stimulated systems, all IP_3R channels are presumably sensitized, and this justifies our treatment of IP_3 as a parameter. The model equations are:

$$\begin{aligned} \frac{dx}{dt} &= \frac{A_{cm}}{V_{cyt}}(J_{in} - J_{out}) + \frac{A_{ER}}{V_{cyt}}(J_{ER\_out} - J_{ER\_in}) + \frac{A_{gap}}{V_{cyt}} J_{gap} \\ \frac{dz}{dt} &= \frac{A_{cm}}{V_{cyt}}(J_{in} - J_{out}) + \frac{A_{gap}}{V_{cyt}} J_{gap} \end{aligned} \tag{2}$$

where A_{cm}, A_{ER}, A_{gap} are the total areas of the plasma membrane, the ER membrane and the gap junctions, respectively.

A schematic drawing of the model is shown in Fig. 1. Calcium is exchanged between the cytosol and a single, uniformly distributed ER compartment. The Ca^{2+} release through the ER membrane (J_{ER_out}) is through calcium-induced calcium release (CICR) activated by IP_3 and is given by a two-variable model ($x;IP_3$) as

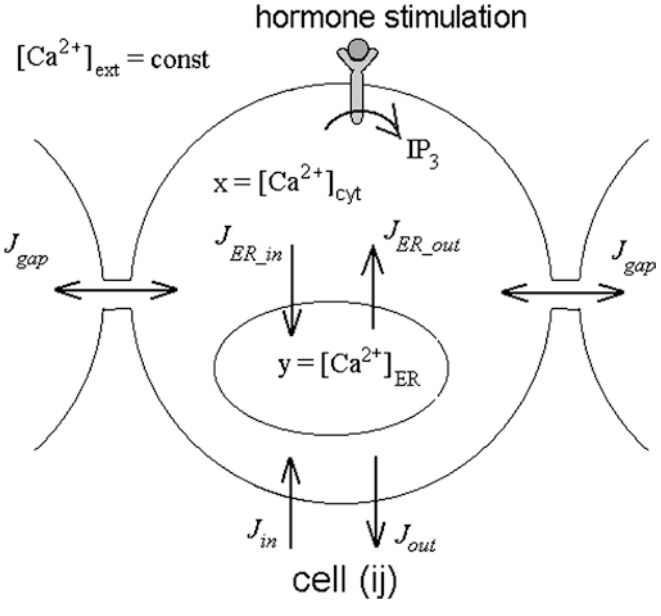

Fig. 1 Flow diagram of calcium fluxes. The model variables and Ca^{2+} exchange across the cell boundary and ER membrane are shown

proposed by Li and Rinzel (1994). Re-uptake of Ca^{2+} in the ER (J_{ER_in}) occurs by Ca^{2+}-ATPases. Similar pumps on the plasma membrane deplete Ca^{2+} from the cytosol (J_{out}). Finally, Ca^{2+} influx across the plasma membrane (J_{in}) takes place through store-operated calcium channels (SOCCs). In accordance with the scheme suggested by Dupont and Goldbeter (1993), it is taken to be controlled by the level of IP_3 in the cell. Thus, the ER store becomes depleted with increasing hormone stimulation. Details of the model functional expressions are provided in the Appendix.

To simulate a physical cell layer, we place each cell with the internal Ca^{2+} dynamics (Eq. 2) on a two-dimensional grid. Cells are connected to their nearest neighbours by gap junction channels and the Ca^{2+} flux (J_{gap}) is assumed to be diffusion controlled, neglecting any electrical potential differences between the cells:

$$J_{gap} = \sum_{\text{neighbours}} p_n(x_n - x_{ij}) \text{ where}$$
$$n = (i-q, j), (i+1, j), (i, j+1), (i, j-1) \tag{3}$$

The total flux is a sum of the fluxes between cell ij and its four nearest neighbours with subscript n. The term $p_{ij,n}$ is the permeability between cell ij and cell n. For simplicity, the permeability is assumed to be constant in time and symmetrical, i.e. $p_{ij} = p_{ji}$. With use of Eqs. (2), (3), the coupling constant $\gamma_{ij,n}$ can be expressed as:

$$\gamma_{ij,n} = \frac{A_{gap,ij-n}}{V_{cyt,ij}} \; p_{ij,n} \tag{4}$$

Finally, three structural parameters are introduced to define the size and shape of the cell and the ER compartment:

$$\alpha = \frac{A_{ER}}{A_{cm}} \quad \beta = \frac{V_{ER}}{V_{cyt}} \quad \rho = \frac{A_{cm}}{V_{cyt}} \tag{5}$$

With these definitions, we arrive at the following equations to describe the temporal and spatial aspects of Ca^{2+} signalling in hormone-stimulated MDCK cells:

$$\begin{aligned}
\frac{dx_{ij}}{dt} &= \rho\left\{ v_l + v_0 \frac{IP_{3ij}}{K_0 + IP_{3ij}} - v_2 \frac{x_{ij}^2}{K_2^2 + x_{ij}^2} \right. \\
&\quad \left. + \alpha_{ij}\left[(c_1 P_{IP3R} + c_2)\left(\frac{z_{ij} - x_{ij}}{ß}\right) - v_1 \frac{x_{ij}^2}{K_1^2 + x_{ij}^2} \right] \right\} \\
&\quad + \sum_{\text{neighbours}} \gamma_{ij,n}(x_n - x_{ij}) \frac{dz_{ij}}{dt} \\
&= \rho\left\{ v_l + v_0 \frac{IP_{3ij}}{K_0 + IP_{3ij}} - v_2 \frac{x_{ij}^2}{K_2^2 + x_{ij}^2} \right\} \\
&\quad + \sum_{\text{neighbours}} \gamma_{ij,n}(x_n - x_{ij}); \\
P_{IP3R} &= \frac{\left(d_2 \frac{d_1 + IP_{3ij}}{d_3 + IP_{3ij}} IP_{3ij} x_{ij} \right)^3}{(d_p + IP_{3ij})^3 (d_a + x_{ij})^3 \left(d_2 \frac{d_1 + IP_{3ij}}{d_3 + IP_{3ij}} + x_{ij} \right)}
\end{aligned} \tag{6}$$

We use cyclic boundary conditions on the grid because we are interested in large-scale phenomena. This particular choice of boundary conditions does not restrain Ca^{2+} flow from edge cells, which communicate on equal terms with all other cells on the grid. The model equations are solved numerically with use of a Matlab programme. A fourth-order Runge-Kutta algorithm is employed in combination with an adaptive step-size algorithm to minimize computational efforts and ensure better accuracy of the solutions. The maximum time step is set to 0.1 s based on preliminary simulations to test the stability of the solutions.

Results

Single-cell calcium oscillations

Agonist-induced Ca^{2+} signalling in MDCK cells is well described experimentally (Rottingen et al. 1997; Jan et al. 1998). Global stimulation with bradykinin in concentrations of between 1 nM–1 μM induces synchronized cytosolic Ca^{2+} oscillations in the cells with frequencies of ~0.5–1 min^{-1}. Noticeably, the periodicity of the oscillations appears to be relatively independent of agonist dose. The primary transient is stronger (~1,000 nM) than the secondary spikes (~500 nM), and the baseline levels are ~150–200 nM. The cells respond heterogeneously to uniform agonist stimulation. Hence, both the internal frequencies and the shape of the oscillations vary markedly in the population. Figure 2A shows synchronous Ca^{2+} signalling in five nearby cells and the average Ca^{2+} level in the experiment (thick line).

With proper parameter adjustments (Table 1), the model can reproduce well the experimental observations of Ca^{2+} oscillations in individual MDCK cells. Cell heterogeneity is introduced in two ways. First, the cells are thought to vary with respect to their hormone sensitivity. This is caused either by different densities of hormone receptors, or by kinetic discrepancy among the receptors and other components of the signalling pathway. The effect is incorporated by varying the IP_3 level in the population. Second, cell structural differences are considered by assigning different α parameter values to the cells. The two other structural variables, β and ρ, are kept invariant in the cell group. In this case, variations in αvalues correspond to changes in the shaping of the ER compartment. However, the physical origin of the structural difference is not important. It is used as a general means to introduce cell morphological heterogeneity in the model.

Some computed solutions of Eq. (6) are shown in Fig. 2B: (B1) the Ca^{2+} level in the cytosol, (B2) the Ca^{2+} level in the ER store and (B3) the phase plots of the variables. The Ca^{2+} level is lowered in the ER compartment during active signalling. This phenomenon arises because Ca^{2+} depleted during the primary transient is only partly replenished. Such behaviour has been

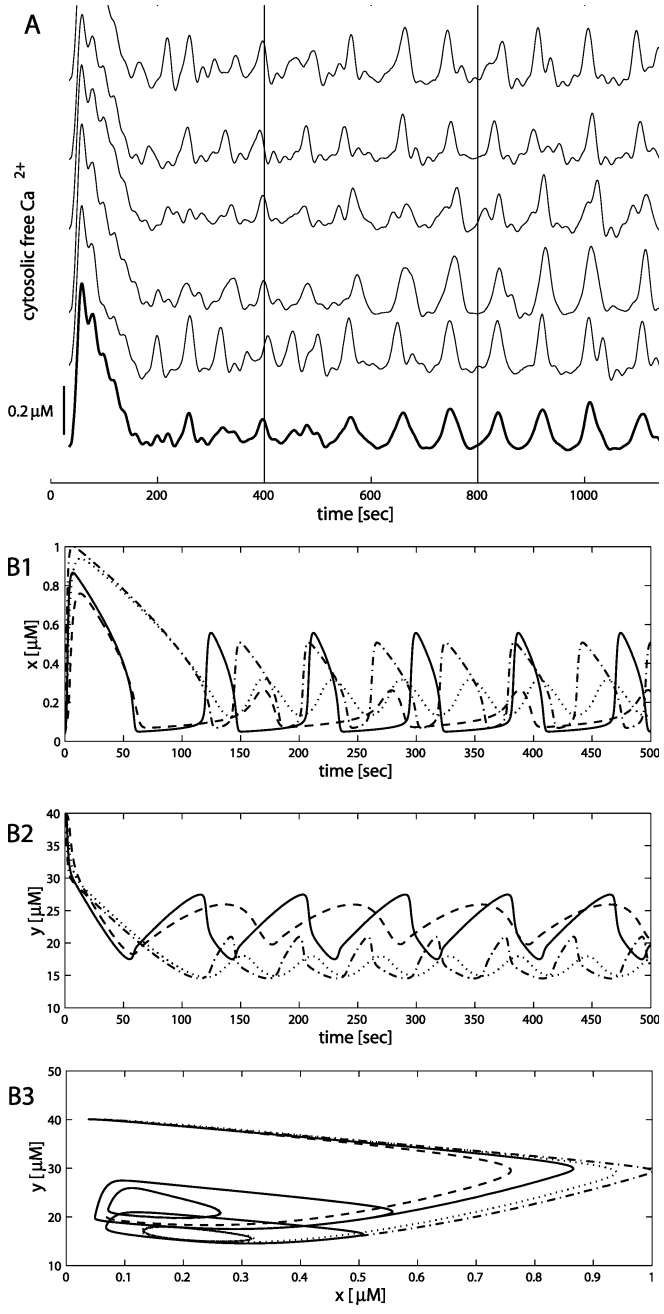

Fig. 2A, B Synchronized calcium oscillations in hormone-stimulated MDCK cells. **A** Experimental data. The time course in cytosolic free Ca^{2+} concentrations of five nearby MDCK cells globally stimulated with bradykinin (50 nM) at time $t = 30$ s. The average Ca^{2+} concentration from the same experiment (*thick line*) is shown *below*. The experiment included a total of 29 cells with constant baseline levels. The synchronization process is not immediate and, in this particular experiment, the average Ca^{2+} level stays elevated during the first ~500 s, indicating that the cells oscillate asynchronously in this period. The single-cell signals are filtered using a fifth-order low-pass elliptic filter. **B** Model simulations of single-cell oscillations. Variability in frequency and shape of **B1** the cytosolic Ca^{2+} spikes, **B2** the changes in ER concentration of free Ca^{2+}, and **B3** corresponding trajectories in the phase plane between the two variables. The plots are generated using different (IP_3, α) values: 1.5 μM, 1.0 (*dashed line*); 1.5 μM, 2.5 (*solid line*); 4.0 μM, 1.0 (*dotted line*); and 4.0 μM, 2.5 (*dashed-dotted line*). Other parameters are listed in the Appendix

reported, though mainly for high hormone stimulation or during prolonged signalling (Shuttleworth 1999).

A certain amount of stimulation must be present in the model for sustained Ca^{2+} signalling to appear. Non-stimulated cells ($IP_3 = 0$) or weakly stimulated cells are in resting states with constant Ca^{2+} levels; the states (x_r,z_r;IP_3,α) are found by equalizing the various fluxes in Eq. (6). When the IP_3 level increases, larger amounts of Ca^{2+} are released from the internal store. At some point, the Ca^{2+} flow into the cytosol will trigger calcium-induced calcium release and formation of a transient. Within the model framework, the system undergoes a supercritical Hopf bifurcation, whereby the steady state becomes unstable and is replaced by a stable limit cycle solution (Fig. 2C). As the IP_3 level is further increased, the Ca^{2+} level in the ER drops until finally it becomes too low to support transient formation. At this point, the model dynamics experiences a second supercritical Hopf bifurcation, whereby stability is passed back to a steady state from the oscillatory solution. This steady state is characterized by a low Ca^{2+} concentration in the ER store compared with the level in a non-stimulated cell. The bifurcation points depend on the cell structure and are found from linear stability analysis to occur at $IP_3 = 1.313$ and 4.715 μM for $\alpha = 1.0$, and $IP_3 = 0.765$ and 5.725 μM for $\alpha = 2.5$.

Single-cell parameter variations

Changes in hormone sensitivity and cell structure affect the Ca^{2+} spiking pattern (Fig. 3). The hormone sensitivity has a relatively strong influence on the periodicity (Fig. 3A) and half-width (Fig. 3C) of the signal. Both the frequency and half-width increase with increasing IP_3 level. In contrast, the α parameter mainly affects the amplitude of the oscillations (Fig. 3B). High α values produce oscillations with high amplitudes.

In the simulations to follow, the cells were assigned different α levels ($1.0 \le \alpha \le 2.5$) and IP_3 levels ($1.35\ \mu M \le IP_3 \le 4.0\ \mu M$) and exclude the region close to the upper bifurcation. In laboratory experiments, it is possible to reach this bifurcation point simply by increasing the agonist dose sufficiently. Nevertheless, these IP_3 concentrations are far above the physiological levels in living tissue. Uniform distributions of pseudo-random numbers on the specified intervals are generated with use of the Matlab function "rand". The stochastic assignment produces a non-homogeneous population of oscillators that differ in periodicity (55–110 s), amplitude (300–600 nM) and half-width (20–30 s) in agreement with the experimental data.

Intercellular calcium signalling

We now model synchronization of Ca^{2+} signalling in a heterogeneous population of cells. We couple the

Table 1 Table of model parameters

Parameter	Symbol	Value	Reference
Rate constant of calcium leak from ER	c_1	40 s^{-1}	Fitted to experiment
Rate constant of calcium release through IP_3R	c_2	0.02 s^{-1}	Fitted to experiment
Constants for the opening probability, P_{IP_3R}, of IP_3R channels	d_1	0.3 μM	(Li and Rinzel 1994) Determined experimentally
	d_2	0.4 μM	(Li and Rinzel 1994) Determined experimentally
	d_3	0.2 μM	(Li and Rinzel 1994) Determined experimentally
	d_a	0.4 μM	(Li and Rinzel 1994) Determined experimentally
	d_p	0.2 μM	(Li and Rinzel 1994) Determined experimentally
Half-maximal calcium extrusion at ER membrane	K_1	0.12 μM	(Moraru et al. 1999) Determined experimentally
Maximal calcium extrusion rate at ER membrane	v_1	9.0 μM s^{-1}	Fitted to experiment
Half-saturation constant for hormone-dependent calcium entry	K_0	4.0 μM	Mathematical models (Dupont and Goldbeter 1993; Sneyd et al. 1995a)
Maximal hormone-dependent calcium entry rate	v_0	4.0 μM s^{-1}	Fitted to experiment
Calcium leakage rate across cell membrane	v_1	0.15 μM s^{-1}	Fitted to experiment
Half-saturation constant for calcium extrusion	K_2	0.12 μM	(Camello et al. 1996) Determined experimentally
Maximal calcium extrusion rate	v_2	3.4 μM s^{-1}	Fitted to experiment
Structural parameter, see text	β	0.1	Mathematical model (Hofer 1999)
Structural parameter, see text	ρ	0.02 μm^{-1}[a]	(Allbritton et al. 1992) Determined experimentally

[a]The ρ parameter is given in units of μm^{-1}, but is taken dimensionless as the unit has been incorporated in the rate constants of the model equations

individual oscillators by gap junctions ($\gamma \neq 0$) and apply a constant coupling term to all cells on the grid. Simulations are performed on systems of size $N \times N$, where $2 \leq N \leq 25$.

In order to obtain a general idea of the rich system behaviour, it is useful to describe the system at three different levels: (1) a microscopic level in terms of individual cells, (2) a local level defined by the nearest adjacent cells and (3) at a global level.

We express the frequency in terms of angular frequency, i.e. $\omega_{ij} = 2\pi f_{ij}$, with the purpose of tracking the phase relations between cells. At the microscopic level, the transient tops in the N^2 time series are identified and the time they occur, i.e. for all M_{ij} transients, we find the corresponding peaking times $t_{ij}^{\text{peak}} = \left\{ t_{ij}^1 \ldots\ldots, t_{ij}^{M_{ij}} \right\}$. Then we define an instant phase θ_{ij} by

$$\theta_{ij} = 2\pi \frac{t - t_{ij}^m}{t_{ij}^{m+1} - t_{ij}^m} \quad t \in \left[t_{ij}^m; t_{ij}^{m+1} \right[\tag{7}$$

We may use Eq. (8) to define an average frequency as

$$\overline{\omega}_{ij} = \lim_{T \to \infty} \frac{1}{T} \int_0^T \dot{\theta}_{ij}(t) dt \approx \frac{2\pi}{M_{ij}} \sum_{m=1}^{M_{ij-1}} \frac{1}{t_{ij}^{m+1} - t_{ij}^m} \tag{8}$$

Furthermore, we will adopt the definitions of macroscopic phase deviation P and global average frequency Ω from Zheng et al. (1998):

$$P = \frac{1}{N^2} \left| \sum_{i=1}^{N} \sum_{j=1}^{N} \exp\left(i\theta_{ij}\right) \right| \quad \Omega = \frac{1}{N^2} \sum_{i=1}^{N} \sum_{j=1}^{N} \overline{\omega}_{ij} \tag{9}$$

where, i appearing in the exponential function is the imaginary unit. The positive quantity P has values between 0 and 1, where $P = 1$ indicates complete phase synchronization. For $\gamma < \gamma_c$, the phase deviation will vary in time and accordingly we will also study its time average $\langle P \rangle$:

$$\langle P \rangle = \lim_{T \to \infty} \frac{1}{T} \int_0^T P(t) dt \approx \frac{1}{T - t'} \int_{t'}^T P(t) dt \tag{10}$$

Equations (10) and (11) are defined for a population of phase oscillators, where the phase advances uniformly

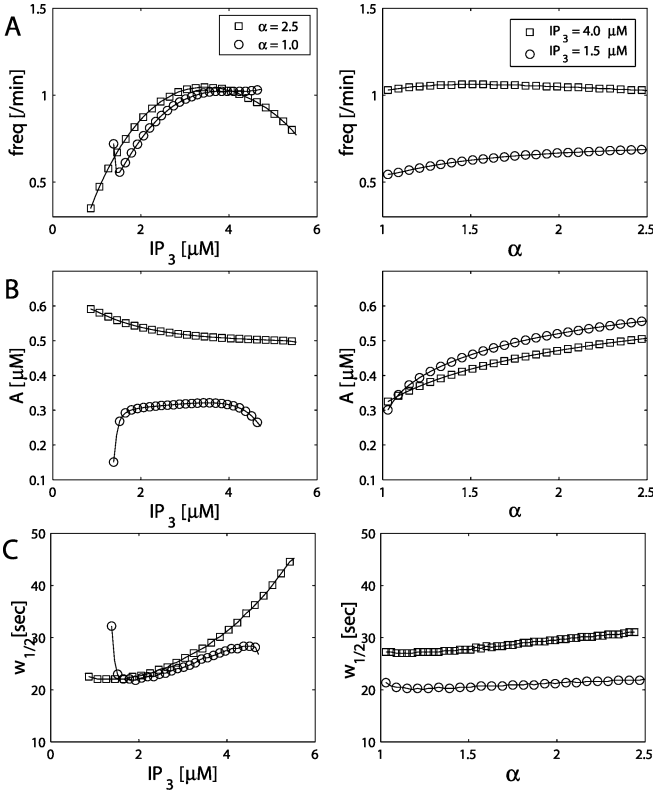

Fig. 3A–C Model solutions and single-parameter variations and oscillation characteristics. Single-cell oscillatory characteristics plotted as function of IP_3 (*left column*) and α (*right column*): **A** frequency, **B** amplitude, and **C** time duration of each spike defined by its half-maximum width. All other parameters as listed in the Appendix

between oscillation peaks. However, the oscillations in the present context are characterized by their amplitudes. The equations are therefore approximate and rest on the assumption of constant phase velocity between two consecutive peaks (Eq. 8). When local behaviour is studied, the sums in the equations are replaced with the sums over the nearest and next-nearest neighbours. The term "natural frequency" will be used throughout the text. It refers to the frequencies of oscillation in single cells with no coupling (i.e. the frequencies of endogenous oscillations).

Critical coupling

Hofer (1999) modelled synchronization between two- and three-gap junctionally connected hepatocytes. Frequency variations (29 s–4.6 min) were imposed by changes in either IP_3 or one of the structural parameters β and ρ. He found that the change from non-synchronous to synchronized signalling occurs at a critical Ca^{2+} permeability, and that the point of transformation depends on the frequency difference between the cells.

In the two-dimensional extension of the model with random IP_3 and α values, we recover the existence of a critical gap junctional coupling γ_{crit}, which must be exceeded before periodic intercellular waves emerge. Figure 4 shows time snapshots of the global signalling pattern for various degree of coupling ($N=15$). The uncoupled cells oscillate with their natural frequencies, which generates a random spiking pattern (Fig. 4A). Local clusters of simultaneous spiking clusters appear in weakly coupled systems (Fig. 4B, C). For $\gamma=\gamma_{crit}$, the population of oscillators form a functional continuum (Fig. 4D, E).

We plot the global phase deviation $\langle P\rangle$ as function of the coupling (Fig. 5A). The critical coupling is manifest as a sudden change—or discontinuity—in $\langle P\rangle$. The phase-locking transition does not cause the population to oscillate synchronously in a strict physical sense, i.e. $\langle P\rangle < 1$. Typically, we find that $\langle P\rangle \geq 0.65$ for $\gamma \geq \gamma_{crit}$. Thus, the phase-lag between the front and the tail of the intercellular wave is, at most, 2.5 rad. Representative examples of the Ca^{2+} signalling pattern for different γ values are shown in Fig. 5B.

Characterizing the oscillations

In Fig. 6 we plot the global frequency, amplitude and signalling strength ($\bar{\omega}_{ij}$, $\bar{A}_{ij}$, S_{ij}) as function of γ. Each of the N^2 cells is represented by a mean value from the time series, e.g. we obtain N^2 components in the range $(\min(\bar{\omega}_{ij}),\ldots,\max(\bar{\omega}_{ij}))_{\gamma}$. We make a bar plot of these extremes, together with the average value $(\Omega)_{\gamma}$. Three horizontal lines indicate the corresponding global extremes and mean values of the isolated oscillators, e.g. $(\min(\bar{\omega}_{ij}), \Omega, \max(\bar{\omega}_{ij}))_{\gamma=0}$.

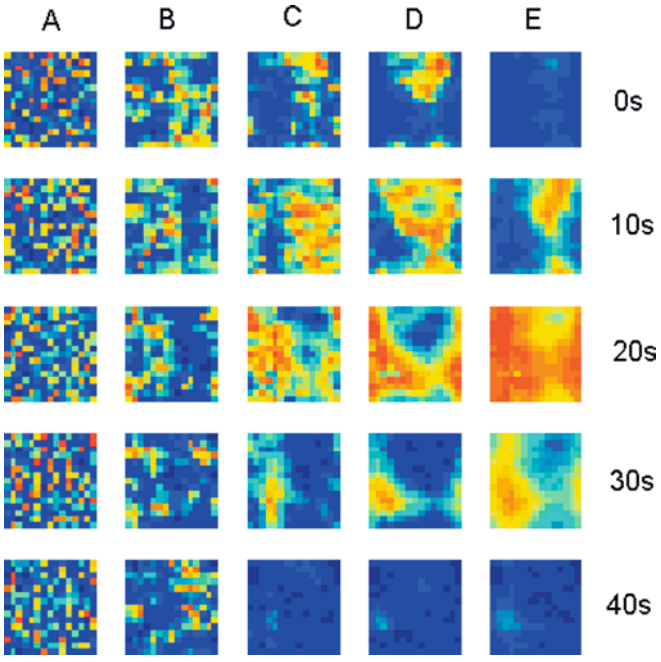

Fig. 4A–E Calcium signalling for variable coupling. Pseudo-colour images of global Ca^{2+} signalling for various degrees of coupling. The coupling increases from *left* to *right*, and the direction of time is downwards in intervals of 10 s: **A** $\gamma=0\ s^{-1}$; **B** $\gamma=0.02\ s^{-1}$; **C** $\gamma=0.04\ s^{-1}$; **D** $\gamma=0.08\ s^{-1}$; **E** $\gamma=0.16\ s^{-1}$. Clustering is visible from **C** onwards. In **D, E**, the coupling is above γ_{crit}. The simulations are made with the same 15×15-sized grid, so that each cell is randomly assigned with identical (IP_3, α) parameter values in the different runs. One pixel corresponds to one cell

The critical coupling is visible as the point where $\min(\bar{\omega}_{ij})$ and $\max(\bar{\omega}_{ij})$ collapse onto the average global frequency Ω (Fig. 6A). The global frequency at the critical coupling is close to the frequency of the oscillator with the highest natural frequency. The result is consistent with the one obtained by Hofer (1999) in the case of two coupled cells. Another point of interest is that Ω increases when γ is raised above zero to a value that is higher than $\max(\bar{\omega}_{ij})_{\gamma=0}$ before it stabilizes. As will become apparent shortly, these high-frequency oscillations below γ_{crit} are expressions of chaos. Above γ_{crit}, the average frequency approaches $(\Omega)_{\gamma=0}$ asymptotically (data not shown). Hence, the mixed oscillators—with no spatial ordering in their frequency—synchronize at an intermediate frequency provided the coupling is large enough.

Below γ_{crit}, the maximal amplitude $\max(\bar{A}_{ij})$ decreases with increasing coupling (Fig. 6B). This is intuitively clear: Ca^{2+} will leak from spiking cells into their out-of-phase neighbours. The leakage also causes formation of minor transients, which explains the concurrent appearance of low-amplitude oscillations. Above γ_{crit}, the minimal amplitude $\min(\bar{A}_{ij})$ increases with increasing Ca^{2+} exchange and $\langle\bar{A}_{ij}\rangle \rightarrow \langle\bar{A}_{ij}\rangle_{\gamma=0}$. Throughout, $\bar{A}_{ij}$ is highly dispersed. Thus, cell differences (cell fingerprints) persist (cf. Fig 1).

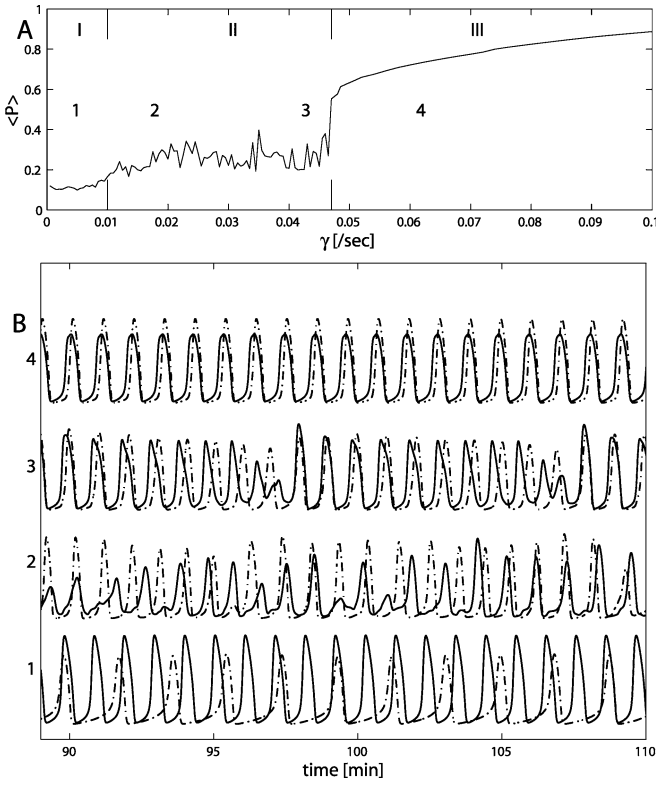

Fig. 5A, B Global phase deviation and critical coupling. **A** Time-averaged global phase deviation $\langle P \rangle$, defined in Eq. (11), plotted versus coupling. The critical coupling is seen as a discontinuity in $\langle P \rangle$ for γ_{crit} 0.046 s^{-1}. The fluctuations below γ_{crit} are caused mainly by a finite time of integration in the simulations. **B** Representative signalling patterns of two single cells for varying γ. The coupling is increasing from **B1–4**, and the signals are referenced in **5B** at their proper γ value. The grid size is 6×6

Chaotic oscillations

Many of the global characteristics are reproduced at the individual level (Fig. 6C, D). The bar plot shows the extremes and mean values of time-series from two single cells, e.g. $(\min(\omega),\bar{\omega},\max(\omega))$. Of special interest, we find highly time-dependent and complex spiking patterns for intermediate coupling (cf. Fig. 5B2).

Are the fluctuating frequencies below γ_{crit} chaotic? We plot the return map of $\omega(n)$ versus $\omega(n+1)$ of a cell for four different couplings (Fig. 7A–D). In this plot, periodic solutions give rise to a finite number of dots, for example, a period-1 solution will show up by a single dot. Positive maximal Lyapunov exponents ($\lambda > 0$) confirm the existence of chaotic behaviour in the region (Fig. 7E). Chaos is prevailing for $\gamma > 0.012$ s^{-1} (Fig. 7B–D) and is not found for all subcritical γ-values. Similar coupling-induced chaos has been reported in systems of phase oscillators with nearest coupling (Zheng et al. 1998).

The synchronization process

Based on the previous discussion, we separate the system dynamics into three different regimes (I–III) as the coupling is increased and the oscillators are led to synchronization (see Fig. 5A). At one end, we have the phase-locking transition at γ_{crit}. At the other end, we have a more loosely defined "chaotic coupling", γ_{chaos}, where the periodic behaviour breaks down to be replaced by quasi-periodic and chaotic oscillations.

Case I: $0 < \gamma \leq \gamma_{chaos}$

In weakly coupled systems, the cells influence each other, but not to the extent that they become mutually entrained. The region is characterized by an increase in average frequency, both at the individual and global level, whereas the amplitude diminishes. The growing heterogeneity in the signals is accompanied by a gradual loss of single-cell oscillatory characteristics (Fig 5B1).

Case II: $\gamma_{chaos} < \gamma \leq \gamma_{crit}$

Around the coupling for which $\Omega \max(\bar{\omega}_{ij})_{\gamma=0}$ (Fig. 6A), all global averages (Ω, $\langle A_{ij} \rangle$,$\langle S_{ij} \rangle$) stabilize. Instead, the individual oscillators express highly complex and chaotic spiking patterns (Fig. 5B2). Externally imposed transients of small amplitude appear in the signals. These oscillations deviate from the multiply-periodic orbits that have been found in a two-cell study of coupled non-identical Ca^{2+} oscillators (Bindschadler and Sneyd 2001). Thus, the two-dimensional system appears to possess qualitative properties, which are not generic, with only few interacting cells.

Increasing Ca^{2+} exchange between cells leads to clustering in the signals. We can visualize this process by plotting $\bar{\omega}_{ij}$ for each cell as a function of γ (Fig. 8). Cluster formations are seen when the frequencies merge together to form a branching tree. In general, the cells belonging to local cluster do not become entrained. Hence, the "local" intercellular wave does not appear to have a point of origin. This so-called phase trapping, where the phases are locked only in an average sense, has been reported in studies of coupled oscillators with a phase gradient (Ermentrout and Kopell 1984). However, in a few cases, we have found what appear to be truly phase-locked clusters, but owing to finite time of integration, their existence cannot be established.

Just below γ_{ij}, there are only two clusters left. The cells are locked in oscillation cycles with different periods (Fig. 5B3). In one cluster, the cells may undergo five oscillations, whereas cells in the other cluster experience six oscillations during the same time (5:6). As we approach γ_{ij}, the repeated patterns contain increasing numbers of transients, e.g. (5:6) → (11:12) etc.

Case III: $\gamma > \gamma_{crit}$

The critical coupling marks the transition from local dominance to a situation dominated by long-range interactions. At this point, $\Omega \approx \max(\bar{\omega}_{ij})_{\gamma=0}$, the individual oscillators entrain (1:1) (cf. Fig. 5B4). The

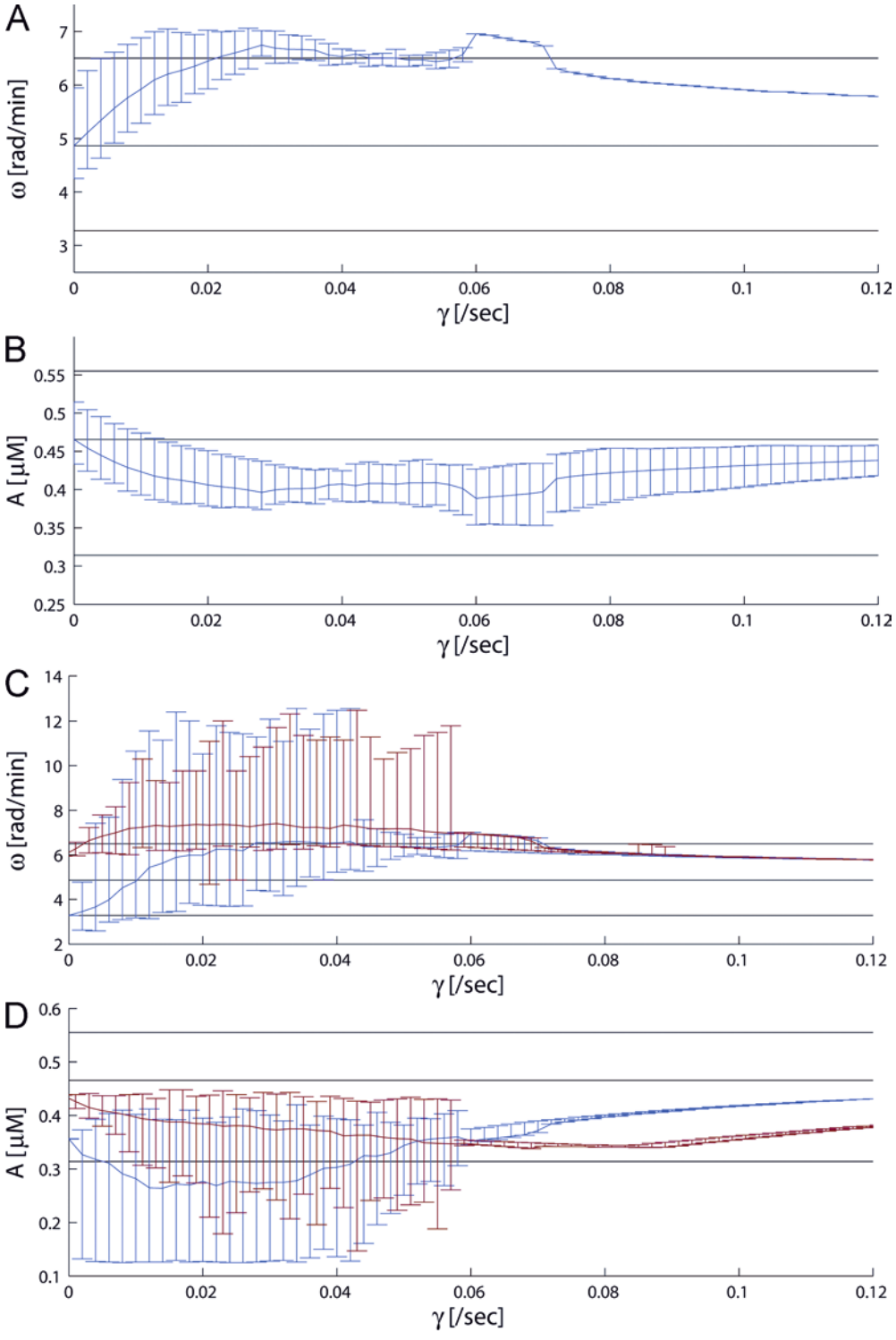

Fig. 6A–D Signalling characteristics for various degrees of coupling. **A** Global frequency plotted as function of time. The plot is made from statistics of complete single-cell time series. Each cell is represented by its mean frequency ($\bar{\omega}_{ij}$) . The plots show the span between minimum and maximum values, i.e. $(\min(\bar{\omega}_{ij}), \langle\bar{\omega}_{ij}\rangle = \Omega, \max(\bar{\omega}_{ij}))_\gamma$. To assist with the interpretation, global extreme and mean values at $\gamma = 0$ are shown with *horizontal bars*. **B** Global amplitude plotted as a function of time. Each cell is represented by its mean amplitude (A_{ij}). Minimal and maximal values from the grid are shown together with the mean, i.e. $(\min(A_{ij}), \langle A_{ij}\rangle, \max(A_{ij}))_\gamma$. Again, the extreme and mean values of the uncoupled system are shown with *horizontal bars*. **C** Single-cell statistics of frequency from two randomly chosen cells (*red* $\alpha = 2.01$; $IP_3 = 3.42$ μM; *blue* $\alpha = 1.34$; $IP_3 = 2.77$ μM) plotted as a function of γ. The plot shows mean, minimum and maximum values of the time series, i.e. $(\min(\omega_{ij}), \bar{\omega}_{ij}, \max(\omega_{ij}))_\gamma$. The *horizontal lines* are similar to **A**. **D** Single-cell statistics of amplitude plotted as a function of γ. The plot shows $(\min(A_{ij}), A_{ij}, \max(A_{ij}))_\gamma$, and the *horizontal lines* are similar to **B**. Simulations are from a 7×7-sized grid; the critical coupling is $\gamma_{crit} \approx 0.06\ s^{-1}$. The simulation was run for 20,000 s to obtain stable averages

oscillations pass through a transitory state before their frequency and their amplitude become constant. Just above γ_{crit}, the transitory state may cover 10–15 periods of oscillation (corresponding to the kink in Fig. 6A between $0.06\ s^{-1} < \gamma < 0.07\ s^{-1}$), where the cells resist for some time before they finally surrender to a common mode. In this situation, the common frequency will be elevated. When γ is further increased, the transitory state shortens and finally the synchronization becomes almost instantaneous, which simultaneously causes the common frequency to be reduced. Well above γ_{crit}, the frequency of the intercellular signalling is reduced, while the population of oscillators express signals that look increasingly similar. As $\gamma \to \infty$, both the frequency and amplitude of the cells approach the averages of the original, uncoupled model.

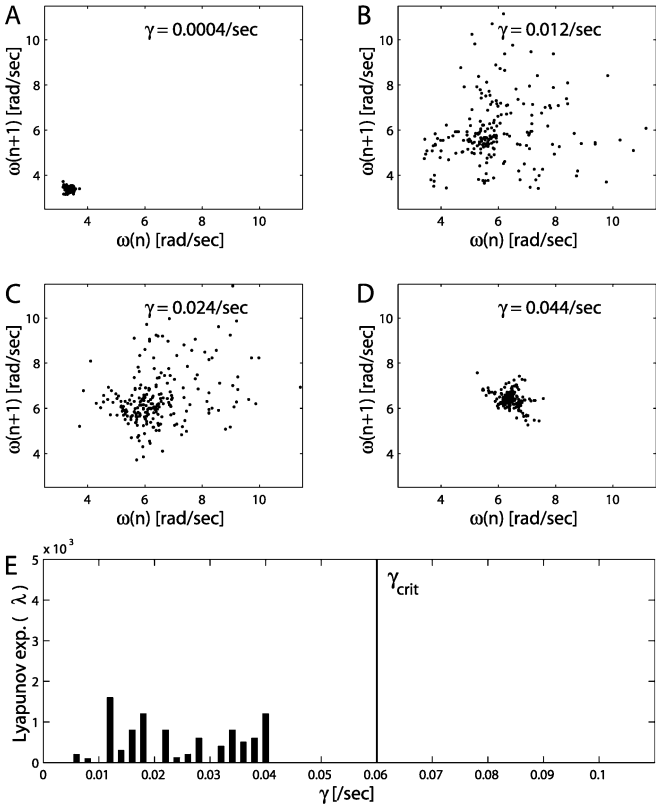

Fig. 7 Chaotic solutions. **A–D** Return maps of a single cell describing the frequency of period n towards the frequency of period $n+1$, i.e. $\omega(n) \rightarrow \omega(n+1)$ for four different couplings. **E** Maximal Lyapunov exponent (λ) versus γ for the same cell. Lyapunov exponents are calculated with use of the Tisean software package, which is available at http://www.mpipks-dresden.mpg.de/~tisean. The method considers the data as a trajectory in embedding space (see Hegger et al. 1999). The distance $\Delta_0 = s_n - s_{n,}$ between a visited point s_n and a very close return to the point s_n should grow exponentially in time, i.e. $|\Delta_m| \approx \Delta_0 \exp(\lambda m)$, then λ is the maximal Lyapunov exponent. The cell is from the same 7×7-sized grid as described in Fig. 6. The simulations cover 30,000 s, which includes about 500 periods of oscillation

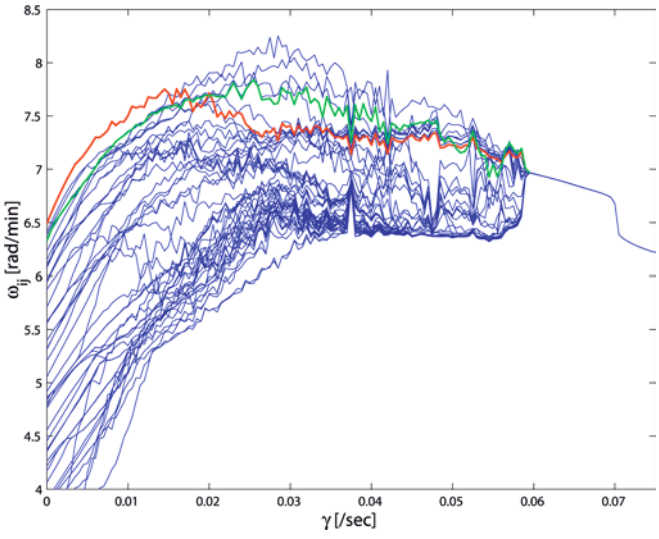

Fig. 8 Branching tree. The average frequency $\bar{\omega}_{ij}$ of 49 individual cells from a 7×7 matrix is plotted as a function of γ. Each line corresponds to one cell. The frequency profiles of the cell with the fastest natural frequency and the pacemaker cells are highlighted in *red* and *green*, respectively. The graph is made on the same system that is shown in Fig. 6. The simulation time is 30,000 s to obtain stable averages, and the resolution is 0.0005 s^{-1}

Pacemaker cells

We define the "pacemaker" cell as the most phase-advanced cell for $\gamma > \gamma_{crit}$. The pacemaker is always found among the oscillators with the highest natural frequencies. However, it is *not* necessarily the cell with $(\bar{\omega}_{ij})_{\gamma=0}$ that acts as pacemaker in the globally connected system (see Fig. 8). A similar finding has been reported previously, albeit in the context of sinoatrial pacemaker synchronization (Michaels et al. 1987). Note that both cells show a frequency increase in weakly coupled systems in accordance with the general trend. The important observation to make is that when $\gamma < \gamma_{crit}$, the pacemaker does not stand out as the cell with the fastest frequency. Thus, the identity of the pacemaker is visible only above γ_{crit} when this particular cell becomes phase-advanced over all other cells on the grid.

Local analysis, including nearest neighbours and next-nearest neighbours, reveals that the pacemaker is surrounded by a "supporting environment", i.e. by cells that oscillate faster (Fig. 9A) and with stronger signalling strengths (Fig. 9B) compared to the cell with $(\bar{\omega}_{ij})$.

Estimation of critical gap junction permeability

The critical coupling increases with the size of the grid, although there are statistical fluctuations in γ_{crit} due to the random parameter assignment (data not shown). Apart from a clear small-scale effect for $N = 2, 3$, which is caused by the cyclic boundary conditions, the increase is relatively small (~0.002 s^{-1} for each unit increase in N). Thus, the solutions on small and large grids are of the same type, if the coupling strength is scaled appropriately. The result coincides with previous findings (De Vries and Sherman 2000), where a linear increase in γ_{crit} with increasing matrix diameter has been derived by a scaling argument.

We can calculate the total gap junctional permeability from Eq. (4):

$$A_{gap}P_n = \gamma_{crit} V_{cyt}\left(1 + \frac{b_{tot}}{K_d}\right) \approx \frac{4\pi}{3} r^3 \gamma_{crit}\left(1 + \frac{b_{tot}}{K_d}\right) = 2.95 \cdot 10^{-9} \mathrm{cm}^3/s \qquad (11)$$

In the calculation, the buffer effect is incorporated by re-scaling V_{cyt} with a factor $(1 + b_{tot}/K_d)$; it is set to 100 in accordance with Allbritton et al. (1992). We use $\gamma_{crit} = 0.05$ s^{-1}; the cell volume is considered spherical with a typical MDCK cell radius of $r = 7.5$ µm, and $V_{cyt} \approx 1/3 V_{tot}$. The estimate of critical permeability is larger than the value found by Hofer (1.36×10^{-9} cm^3/s), but within range of the permeability of tetraetylammonium

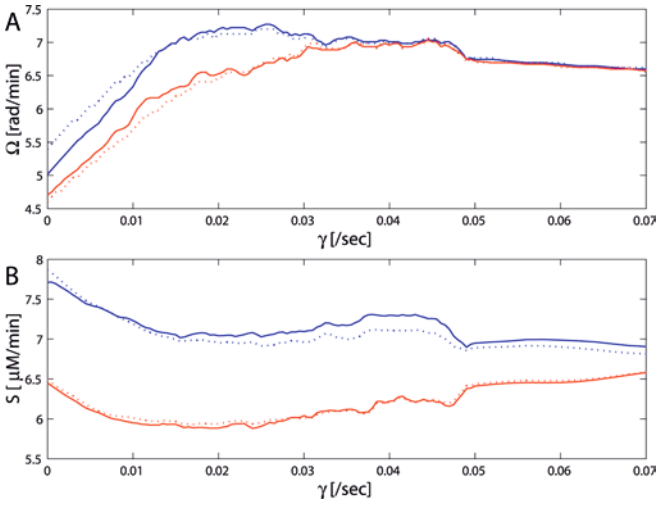

Fig. 9A, B Nearby cells of a pacemaker and fastest oscillator without coupling. **A** The average frequency $\Omega = \langle \bar{\omega}_{ij} \rangle$ plotted as function of γ for cells neighbouring the pacemaker (*blue*) and the cell with fastest natural frequency (*red*). *Solid line*s correspond to the average from the four nearest neighbours; *dashed lines* include the 12 nearest and next-nearest cells. **B** Average signalling strengths $\langle S_{ij} \rangle$ plotted as function of γ. It is defined as: $S = \frac{1}{T-t'} [\int_{t'}^{T} x(t)dt - x_{\text{baseline}}(T-t')]$, where the lower integration limit, t', is set to 200 s to exclude the primary strong transient, and the upper limit, T, is set by the simulation time. The term x_{baseline} is the resting Ca^{2+} concentration in the cytosol. The symbol code is the same as in **A**. Simulations are made on a 10×10-sized grid, and the critical coupling is $\gamma_{\text{crit}} = 0.048\ s^{-1}$

ions in blastomere cells (1–3×$10^{-9}$$cm^3$/s) (Verselis et al. 1986). Using A_{gap}, 7,100 nm^2, we find the critical permeability to be p_n, 0.41 μm. This value can be compared with estimates of IP_3 permeability by Dupont et al. (2000) (0.88 μm/s) and Sneyd et al. (1995b) (2 μm/s).

Synchronization in partly sensitized cell layers

Cells respond heterogeneously to the same hormone stimulus. In experiments with tissue cultures, it is often found that not all stimulated cells oscillate autonomously. This is likely to occur also in living tissue. Thus, it is interesting to study the collective behaviour of the oscillators in these situations.

With this purpose in mind, we placed quiescent cells in random positions on the grid. The cells are partly sensitized, i.e. they do not oscillate on their own, but have $IP_3 > 0$. Thus, they can display high-amplitude Ca^{2+} signalling, but rely on junctional Ca^{2+} inflow to do so (Fig. 10A). In weakly coupled systems, these cells express characteristic low-frequency transients (Fig. 10A1). As we increase γ, the cells oscillate with higher frequencies (Fig. 10A2, 3), until finally the cells keep pace with the other cells (Fig. 10A4). Figure 10B shows experimental Ca^{2+} signals, which show behaviour in common with Fig. 10A1–4.

So what happens to the collective behaviour in these systems? To answer this question, we have constructed a branching tree (Fig. 11A), which is made on the same

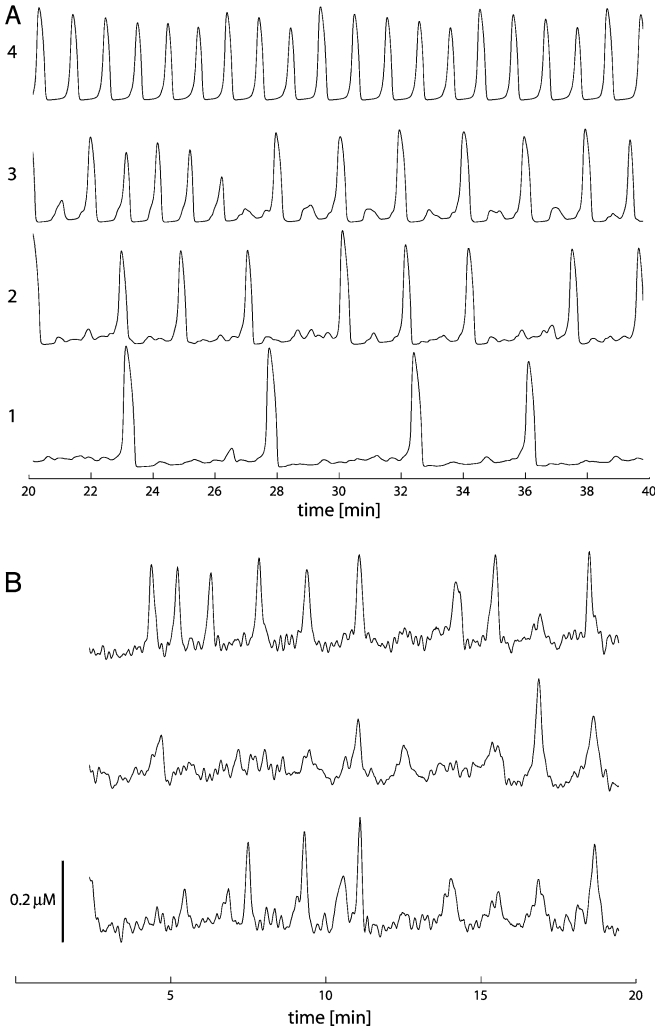

Fig. 10A, B Calcium signalling of partly sensitized cells. **A** Time course of cytosolic Ca^{2+} concentration plotted as a function of time in a partly hormone-sensitive cell ($IP_3 = 0.5$ μM) and for various degrees of coupling (1–4). The coupling increases from *below*: **1** $\gamma = 0.014\ s^{-1}$; **2** $\gamma = 0.35\ s^{-1}$; **3** $\gamma = 0.55\ s^{-1}$; **4** $\gamma = 0.80\ s^{-1}$. The simulations are made on a 7×7-sized grid with quiescent cells ($IP_3 = 0.5$ μM) at a density of 12.5%. The average frequency of the cell versus γ is also shown in Fig. 11A. It corresponds to the quiescent cell that becomes entrained to the slowest cluster at $\gamma = 0.068\ s^{-1}$. **B** Experimental time series from hormone-stimulated MDCK cell layers. The signals are highly irregular and resemble the ones obtained from non-autonomous oscillators in **A**

basic grid as the one in Fig. 8. The density of quiescent cells ($IP_3 = 0.5$ μM) is 12%. First, the presence of quiescent cells causes the critical coupling to increase above the value of the same native grid where all cells oscillate autonomously. Typically, γ_{crit} increases by 20–40% when the density of quiescent cells is 10% (for $IP_3 = 0.5$ μM). However, the extent of the increase in γ_{crit} depends on the particular cells, which become non-autonomous. Second, the quiescent cells entrain with other cells at a different value of coupling, $\gamma < \gamma_{\text{crit}}$. Hence, the cells are up pace with the autonomous cells below γ_{crit}. Third, the pacemaker above γ_{crit} differs, in general, from the pacemaker in the native system. Now,

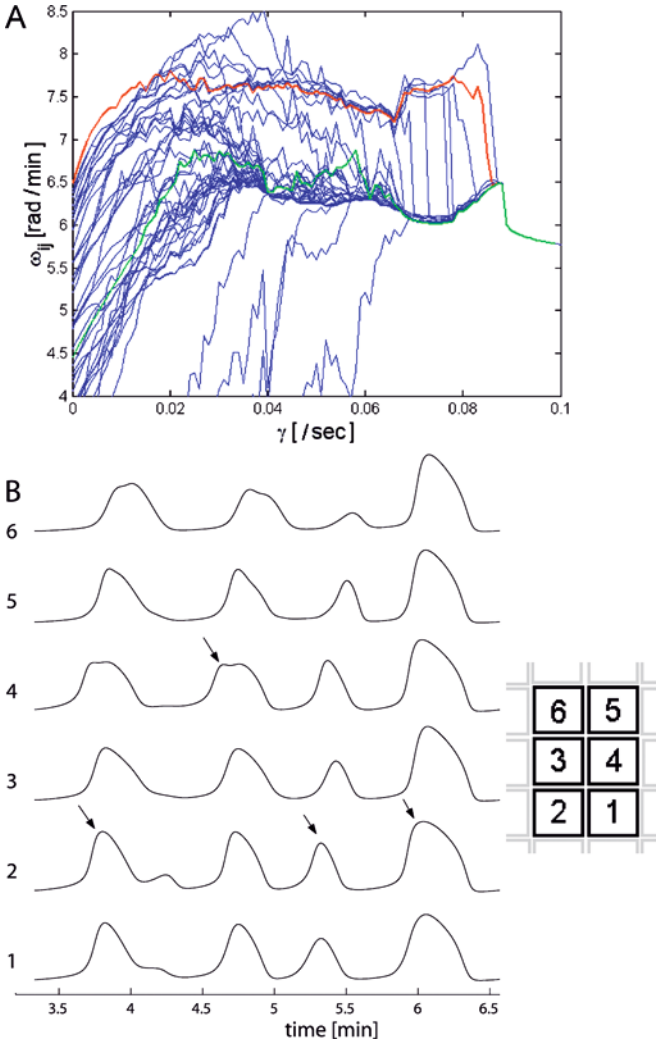

Fig. 11A, B Branching tree of system with quiescent cells. **A** Branching tree constructed from the average frequency $\bar{\omega}_{ij}$ of 49 cells from a 7×7-sized grid. The simulations are performed on the same basic grid as Fig. 8, with four quiescent cells ($IP_3 = 0.5$ μM) for comparison. The cell with the fastest natural frequency and the pacemaker are highlighted in *red* and *green*, respectively. Quiescent cells entrain with a subgroup of cells below γ_{crit}. Note the persistent two-cluster phase ($0.068\ s^{-1} < \gamma < 0.089\ s^{-1}$). **B** The time course of intercellular Ca^{2+} spreading in the fastest-oscillating cluster in **A** at $\gamma = 0.069\ s^{-1}$. The *arrows* show the first spiking cell in a few consecutive oscillations. Note that at each new cycle, different cells take the lead in the signalling. Their physical placement on the grid is indicated on the *right*. The simulation was run for 20,000 s

it will not necessarily belong to the group with the fastest intrinsic frequencies. This, again, underlines the fact that the mode of synchronization is a collective phenomenon. Fourth, quiescent cells act as "buffers", which may fragment the population into smaller groups with different multiply-periodic behaviour below γ_{crit}.

Note the robust two-cluster phase $0.069\ s^{-1} < \gamma < 0.089\ s^{-1}$ in Fig. 11A, where the cells cannot reach a "consensus" as to the spiking frequency. Nevertheless, when we increase γ, the fast oscillators surrender one by one until γ_{crit} is reached. The multiply-periodic behaviour can give rise to a back-firing phenomenon (Fig. 11B), where one local wave proceeds in the opposite direction to the preceding wave. Interestingly, short-distance (four to nine cells) synchronous signalling in ATP-stimulated articular chondrocytes is found to express such retrograde waves (D'Andrea and Vittur 1996).

Above γ_{crit}, the global phase deviation $\langle P \rangle$ will tend to become larger than the corresponding value from the native system (data not shown). Hence, the quiescent cells do not have a will of their own but follow passively the signalling in their neighbourhood.

Discussion

We have used a lattice stochastic model to study large-scale intercellular signal synchronization in renal epithelia. The numerical model is found to agree with empirical observations (PCH) of globally hormone-stimulated MDCK cells in several ways. First, within the model scenario, we find that for $\gamma \approx \gamma_{crit}$, the common frequency of oscillation during synchronous signalling occurs close to the fastest natural frequency, i.e. $\Omega \approx \max(\bar{\omega}_{ij})_{\gamma=0}$. Second, the pacemaker belongs to the subpopulation of cells with the highest natural frequencies. Third, the signal is found to propagate radially from the pacemaker cell (cf. Fig. 4). However, the simulations suggest that the conjecture of a robust pacemaker that literally "sets the pace" of the oscillations in the entire population is not correct: Synchronous signalling does not occur at the command of a few particular cells. Rather, it is an outcome of mutual interactions between the pacemaker and all other cells. In fact, the pacemaker is induced to change its spiking frequency below γ_{crit} just like any other cell. In addition, a cell is not "selected" to be pacemaker based solely on its natural frequency, but perhaps because other fast-oscillating cells nearby render it support.

Intercellular Ca^{2+} signalling has been studied by a number of authors (for a recent review, see Schuster et al. 2002). The present work is a detailed study of large-scale synchronization in epithelia in the particular context of MDCK cells and compares simulation results to experimental data. However, the present model also belongs to a general class of dynamic systems characterized by expressing oscillations with random natural frequencies in the absence of coupling. These systems are common in physiological systems (Winfree 1980; Glass and Mackay 1988; Keener and Sneyd 1998), but are also frequent in chemical and physical systems (Pikovsky et al. 2001). They tend to behave in a generically similar manner, despite many differences in details. Indeed, most of the qualitative behaviour that we present has been reported in other systems of coupled oscillators.

The critical coupling in the simulations tends to increase with each unit increase in N. However, the effect is small and could well be an artefact related to the choice of boundary conditions. In addition, we find large

statistical fluctuations in the γ_{crit} obtained (cf. Fig. 6 with Fig. 9, for example), which relates to the random parameter distribution. The stochastic nature of the model makes it difficult to generalize about the dependence of the solutions on the number of cells on the grid while keeping γ constant. The result will depend intimately on the particular characteristics of these cells and the local environment they encounter.

One interesting finding in this study is the chaotic oscillations for intermediate coupling $0 < \gamma < \gamma_{crit}$. This particular phenomenon is not often mentioned in the literature of intercellular Ca^{2+} signalling. However, in a recent paper concerning a two-cell system (Bindschadler and Sneyd 2001), indications of chaotic behaviour were reported, although no attempt was made to distinguish between chaos and multiply-periodic solutions of high period. The dynamic behaviour of the present model shows a remarkable resemblance to a model representation of coupled laser arrays (Zheng et al. 1998). In both models, the self-sustained oscillators change from periodic to quasi-periodic and chaotic behaviour with increasing coupling, until they return to periodic motions and finally lock onto a single frequency. At present, the physiological relevance of these chaotic oscillations is not clear, and future experimental studies of Ca^{2+} signalling in weakly connected epithelia are needed.

The question of synchronization mode was addressed in a bi-dimensional model, which mathematically resembles the extended Hofer model (Michaels et al. 1987). The study concerned heart pacemaker activity, and the cells were assigned with random intrinsic cycle lengths (290–390 s). In agreement with the present study, the pacemaker was not identical to the cell with the highest internal frequency, but was found to be among the group of fastest oscillators. However, the population entrains at an intermediate period. It is concluded that sinus node synchronization occurs through a "democratic" process, where the cells, through mutual interaction, achieve an agreement as to the firing frequency. In this respect, the current model is more restrictive: true "democracy" is present only for $\gamma >> \gamma_{crit}$, where the frequency approaches the arithmetic mean of the frequencies in the uncoupled system.

Hofer (1999) briefly mentioned weakly responsive cells in his paper. He shows that signal synchronization can be transmitted from one cell to another through an intermediate less responsive cell, provided the IP_3 level of that cell is in the excitable regime (partly sensitized). Our results are consistent with this behaviour. Furthermore, we find that the threshold coupling increases in the presence of quiescent cells, which are being paced by the population to express high-frequency signalling. In these systems, the population is divided into few (usually two) clusters with multiply-periodic behaviour for relatively large coupling intervals below γ_{crit}. This phase is so prominent that one should expect to see such behaviour experimentally.

We analyzed data from bradykinin-stimulated single MDCK cells within local regions (100–150 cells). Although the Ca^{2+} signalling is clearly oriented, we cannot establish global spatial correlation over extended periods of time. Instead, we typically found spatial correlation in local clusters of much smaller size (5–15 cells). The same observation was made with cultured articular chondrocytes (D'Andrea and Vittur 1996). The lack of large-scale spatial correlation could reflect poor gap junctional contact between some parts of the cell layer. Indeed, permeability studies of cultured cells with the use of fluorescent dyes (Lucifer Yellow) show large variability in cell-to-cell conductance (Bennett and Verselis 1992), and some cells fail to establish functional gap junctions under culture conditions (Nilius and Droogmans 2001).

In an experimental situation, we do not know with accuracy the natural frequencies of the cells. Commonly, the intrinsic frequencies are estimated with the use of gap junction blockers such as octanol or 18-α-glycyrrhetinic acid. We find, however, that the junction blockers tend to change the signalling in a qualitative manner, which has similarly been observed in other systems (Moortgat et al. 2000). Instead, we used the early-phase signals to assess the intrinsic frequencies.

We do not consider spatial Ca^{2+} distribution in the cytosol in the present model. Thus, Ca^{2+} entering a cell through gap junctions is assumed to be distributed evenly over the entire volume. Endogenous buffers make Ca^{2+} diffuse slowly in the cytosol (15–65 μm/s) (Rottingen and Iversen 2000), and it is not conceivable that diffusion of Ca^{2+} can drive synchronized signalling in multicellular systems. Instead, it has been argued that Ca^{2+} waves are phase waves where loci of the Ca^{2+} stores act as coupled oscillators (Roth et al. 1995), and diffusion of IP_3 is responsible for setting up a gradient (Jafri and Keizer 1994). In fact, recent studies confirm the existence of strongly coupled Ca^{2+} stores in guinea-pig gastric pylorus (van Helden and Imtiaz 2003). Hence, junctional Ca^{2+} is likely to interact prominently with the ER compartment close to the entrance channel. In this scenario, there are two coupled Ca^{2+} oscillator systems, which together are responsible for the emergence of long-range synchronicity: one is the coupling between individual cells mediated by junctional Ca^{2+} diffusion, the other is the coupling of individual ER membrane loci, which is directed by Ca^{2+} and/or IP_3 diffusion. More realistic models would incorporate such "double layer" mechanisms.

Finally, we studied systems of Ca^{2+} oscillations with no spatial ordering in the natural frequencies. This is exactly what is observed experimentally in cultured MDCK cells. It has been shown that multiplet hepatocytes (Tordjmann et al. 1997, 1998; perfused intact liver cells (Nathanson et al. 1995) and lung capillary cells (Ying et al. 1996) are ordered by a frequency gradient. However, at present, there is no evidence to support the existence of such a gradient in renal epithelia from the collecting duct. It remains to be seen whether

the apparent lack of spatial confinement of pacemakers in this experimental system is observed in the intact tissue, where cells express their proper architectural organization.

Appendix

Model expressions

The expression for the Ca^{2+} release from the ER (J_{ER_out}) is taken from Li and Rinzel (1994):

$$J_{ER\_out} = (c_1 P_{IP3R} + c_2)(y - x) \text{ with}$$
$$P_{IP3R} = \frac{\left(d_2 \frac{d_1 + IP_{3ij}}{d_3 + IP_{3ij}} IP_{3ij} x_{ij}\right)^3}{\left(d_p + IP_{3ij}\right)^3 \left(d_a + x_{ij}\right)^3 \left(d_2 \frac{d_1 + IP_{3ij}}{d_3 + IP_{3ij}} + x_{ij}\right)} \quad (12)$$

where the driving force is the concentration difference ($y = x$). The channel opening probability, P_{IP_3R}, is described by considering three binding sites on each IP_3R subunit: one for IP_3 and one activating and one deactivating Ca^{2+} binding site. The constants c_1 and c_2 are rate constants of the maximal Ca^{2+} channel release and Ca^{2+} leakage from the ER.

The Ca^{2+}-ATPase pumps on the ER membrane (J_{ER_in}) and plasma membrane (J_{out}) are both modelled by simple Hill expressions in cytosolic Ca^{2+} x according to

$$J_{ER\_in} = v_1 \frac{x^2}{K_1^2 + x^2} \quad J_{out} = v_2 \frac{x^2}{K_2^2 + x^2} \quad (13)$$

where v_1 and v_2 are maximal rate constants and K_1^2 and K_2^2 represent the Ca^{2+} pumping for which the activity is half-maximum.

The Ca^{2+} entry rate is given as a sum of a small Ca^{2+} leakage and a store-operated Ca^{2+} influx. The store-operated inflow is controlled by the level of IP_3 in the cell as suggested by Dupont and Goldbeter (1993):

$$J_{in} = v_1 + v_0 \frac{IP_3}{K_0 + IP_3} \quad (14)$$

where v_1 is a small-leak term, v_0 is the maximal flux of Ca^{2+} through the store-operated channel, and K_0 is the Ca^{2+} level for half-maximal pumping activity.

References

Allbritton NL, Meyer T, Stryer L (1992) Range of messenger action of calcium ion and inositol 1,4,5-trisphosphate. Science 258:1812–1815

Bennett MV, Verselis VK (1992) Biophysics of gap junctions. Semin Cell Biol 3:29–47

Berridge MJ (2001) The versatility and complexity of calcium signalling. Novartis Found Symp 239:52–64

Berridge MJ, Bootman MD, Lipp P (1998) Calcium—a life and death signal. Nature 395:645–648

Bindschadler M, Sneyd J (2001) A bifurcation analysis of two coupled calcium oscillators. Chaos 11:237–246

Boyett MR, Honjo H, Kodama I (2000) The sinoatrial node, a heterogeneous pacemaker structure. Cardiovasc Res 47:658–687

Camello P, Gardner J, Petersen OH, Tepikin AV (1996) Calcium dependence of calcium extrusion and calcium uptake in mouse pancreatic acinar cells. J Physiol 490(3):585–593

D'Andrea P, Vittur F (1996) Gap junctions mediate intercellular calcium signalling in cultured articular chondrocytes Cell Calcium 20:389–397

De Vries G, Sherman A (2000) Channel sharing in pancreatic β-cells revisited: enhancement of emergent bursting by noise. J Theor Biol 207:513–530

DiFrancesco D (1991) The contribution of the "pacemaker" current (if) to generation of spontaneous activity in rabbit sinoatrial node myocytes. J Physiol 434:23–40

Dupont G, Goldbeter A (1993) One-pool model for Ca^{2+} oscillations involving Ca^{2+} and inositol 1,4,5-trisphosphate as coagonists for Ca^{2+} release. Cell Calcium 14:311–322

Dupont G, Tordjmann T, Clair C, Swillens S, Claret M, Combettes L (2000) Mechanism of receptor-oriented intercellular calcium wave propagation in hepatocytes. FASEB J 14:279–289

Ermentrout GB, Kopell N (1984) Frequency plateus in a chain of weakly coupled oscillators. SIAM J Appl Math 15:215–237

Glass L, Mackay M (1988) From clocks to chaos—the rhythms of life. Princeton University Press, Princeton

Hassinger TD, Guthrie PB, Atkinson PB, Bennett MV, Kater SB (1996) An extracellular signaling component in propagation of astrocytic calcium waves. Proc Natl Acad Sci USA 93:13268–13273

Hegger R, Kantz H, Schreiber T (1999) Practical implementation of nonlinear time series methods: the TISEAN package. Chaos 9:413

Hofer AM, Curci S, Doble MA, Brown EM, Soybel DI (2000) Intercellular communication mediated by the extracellular calcium-sensing receptor. Nat Cell Biol 2:392–398

HoferT (1999) Model of intercellular calcium oscillations in hepatocytes: synchronization of heterogeneous cells. Biophys J 77:1244–1256

Huser J, Blatter LA, Lipsius SL (2000) Intracellular Ca^{2+} release contributes to automaticity in cat atrial pacemaker cells. J Physiol 524(2):415–422

Isakson BE, Evans WH, Boitano S (2001) Intercellular Ca^{2+} signaling in alveolar epithelial cells through gap junctions and by extracellular ATP. Am J Physiol Lung Cell Mol Physiol 280:L221–L228

Jaffe LF (1993) Classes and mechanisms of calcium waves. Cell Calcium 14:736–745

Jafri MS, Keizer J (1994) Diffusion of inositol 1,4,5-trisphosphate but not Ca^{2+} is necessary for a class of inositol 1,4,5-trisphosphate-induced Ca^{2+} waves Proc Natl Acad Sci USA 91:9485–9489

Jan CR, Ho CM, Wu SN, Tseng CJ (1998) Bradykinin-evoked Ca^{2+} mobilization in Madin Darby canine kidney cells. Eur J Pharmacol 355:219–233

Keener J, Sneyd J (1998) Mathematical physiology. Springer, Berlin Heidelberg New York

Klepeis VE, Cornell-Bell A, Trinkaus-Randall V (2001) Growth factors but not gap junctions play a role in injury-induced Ca^{2+} waves in epithelial cells. J Cell Sci 114:4185–4195

Leite MF, Hirata K, Pusl T, Burgstahler AD, Okazaki K, Ortega JM, Goes AM, Prado MA, Spray DC, Nathanson MH (2002) Molecular basis for pacemaker cells in epithelia. J Biol Chem 277:16313–16323

Li YX, Rinzel J (1994) Equations for InsP3 receptor-mediated $[Ca^{2+}]$i oscillations derived from a detailed kinetic model: a Hodgkin-Huxley like formalism. J Theor Biol 166:461–473

Michaels DC, Matyas EP, Jalife J (1987) Mechanisms of sinoatrial pacemaker synchronization: a new hypothesis. Circ Res 61:704–714

Moortgat KT, Bullock TH, Sejnowski TJ (2000) Precision of the pacemaker nucleus in a weakly electric fish: network versus cellular influences. J Neurophysiol 83:971–983

Moraru II, Kaftan EJ, Ehrlich BE, Watras J (1999) Regulation of type 1 inositol 1,4,5-trisphosphate-gated calcium channels by InsP3 and calcium: simulation of single channel kinetics based on ligand binding and electrophysiological analysis. J Gen Physiol 113:837–849

Nathanson MH, Burgstahler AD, Mennone A, Fallon MB, Gonzalez CB, Saez JC (1995) Ca^{2+} waves are organized among hepatocytes in the intact organ. Am J Physiol 269:G167–G171

Nilius B, Droogmans G (2001) Ion channels and their functional role in vascular endothelium. Physiol Rev 81:1415–1459

Pikovsky M, Rosenblum M, Kurths J (2001) Synchronization: a universal concept in nonlinear sciences. Cambridge University Press, New York

Roth BJ, Yagodin SV, Holtzclaw L, Russell JT (1995) A mathematical model of agonist-induced propagation of calcium waves in astrocytes. Cell Calcium 17:53–64

Rottingen J, Iversen JG. (2000) Ruled by waves? Intracellular and intercellular calcium signalling. Acta Physiol Scand 169:203–219

Rottingen JA, Camerer E, Mathiesen I, Prydz H, Iversen JG (1997) Synchronized Ca^{2+} oscillations induced in Madin Darby canine kidney cells by bradykinin and thrombin but not by ATP. Cell Calcium 21:195–211

Sanderson MJ (1995) Intercellular calcium waves mediated by inositol trisphosphate. Ciba Found Symp 188:175–189

Sanderson MJ, Charles AC, Dirksen ER (1990) Mechanical stimulation and intercellular communication increases intracellular Ca^{2+} in epithelial cells. Cell Regul 1:585–596

Schuster S, Marhl M, Hofer T (2002) Modelling of simple and complex calcium oscillations. From single-cell responses to intercellular signalling. Eur J Biochem 269:1333–1355

Shuttleworth TJ (1999) What drives calcium entry during $[Ca^{2+}]i$ oscillations?—challenging the capacitative model. Cell Calcium 25:237–246

Sneyd J, Keizer J, Sanderson MJ (1995a) Mechanisms of calcium oscillations and waves: a quantitative analysis. FASEB J 9:1463–1472

Sneyd J, Wetton BT, Charles AC, Sanderson MJ (1995b) Intercellular calcium waves mediated by diffusion of inositol trisphosphate: a two-dimensional model. Am J Physiol 268:C1537–C1545

Tordjmann T, Berthon B, Claret M, Combettes L (1997) Coordinated intercellular calcium waves induced by noradrenaline in rat hepatocytes: dual control by gap junction permeability and agonist. EMBO J 16:5398–5407

Tordjmann T, Berthon B, Jacquemin E, Clair C, Stelly N, Guillon G, Claret M, Combettes L (1998) Receptor-oriented intercellular calcium waves evoked by vasopressin in rat hepatocytes. EMBO J 17:4695–4703

van Helden DF, Imtiaz MS (2003) Ca^{2+} phase waves: a basis for cellular pacemaking and long-range synchronicity in the guinea-pig gastric pylorus. J Physiol 548:271–296

Verselis V, White RL, Spray DC, Bennett MV (1986) Gap junctional conductance and permeability are linearly related. Science 234:461–464

Winfree AT (1980) The geometry of biological time. Springer, Berlin Heidelberg New York

Ying X, Minamiya Y, Fu C, Bhattacharya J (1996) Ca^{2+} waves in lung capillary endothelium. Circ Res 79:898–908

Zheng Z, Hu G, Hu B (1998) Phase slips and phase synchronization of coupled oscillators. Phys Rev Lett 81:5318–5321

Zimmermann B, Walz B (1999) The mechanism mediating regenerative intercellular Ca^{2+} waves in the blowfly salivary gland. EMBO J 18:3222–3231